Near anode plasma in the plasma interaction facility at UCLA

IEPC-2013-327

Presented at the 33rd International Electric Propulsion Conference,
The George Washington University, Washington, D.C., USA
October 6–10, 2013

Taylor S. Matlock*, Dan M. Goebel†, and Richard E. Wirz‡
University of California Los Angeles, Los Angeles, CA, 90095, USA

A DC cylindrical discharge plasma column is examined in the region between an upstream anode and an axial, magnetized guide section that delivers the plasma created in the anode region to a target downstream. Radial profiles of the plasma potential, density and temperature are obtained with floating emissive and double probes. An alternative method for double probe implementation is discussed and shown to result in plasma potential profiles closely matching those obtained using a floating emissive probe technique. Plasma profiles measured for a range of magnetic field configurations demonstrate the existence of distinct modes of operation of the plasma source. Time resolved measurements of floating potential with an emissive probe reveal several low frequency oscillations which become significant past a critical magnetic field near 100 Gauss. These measurements are performed to inform analytical and numerical models of the device which is being developed to deliver a stable, well defined plasma to a target surface for plasma-material interaction studies.

I. Introduction

The Plasma interactions (Pi) facility is being developed at UCLA for the testing of advanced, micro-architecture materials[1] for applications in harsh environments, similar to that produced in electric propulsion and pulsed power systems. A 250 A hollow cathode plasma source is integrated with guiding solenoidal magnets running across a vacuum chamber to provide a roughly 3 cm diameter plasma to a downstream target material with target-directed, xenon or argon ion fluxes.

The dynamic interactions between plasmas and materials far from equilibrium are a critical and currently not well understood aspect of electric propulsion (EP) and pulsed power device design. Facilities dedicated to the examination of phenomena arising when materials are exposed to extreme plasma environments are in ongoing use for research vital to magnetic confinement fusion[2–6] and hypersonic vehicles[7,8] among other fields. The Pi facility is unique in its dedicated design to provide long-term exposure of materials to plasma conditions relevant to EP and pulsed power applications. More specifically, the plasma source is being developed to efficiently produce plasmas on argon and xenon of moderate electron temperature (2-10 eV), with plasma densities ranging from 10^{16}-10^{19} m^{-3}, and the potential for studies of both wall material redeposition effects and the resiliency of new materials to high heat flux pulses due to plasma species impingement.

The Pi facility is part of a broader effort including numerical modeling of the plasma, on both global[9] and microscopic[10] scales, as well as the reaction of micro-engineered materials.[11] Dedicated measurements of electron emission from the engineered surfaces are also underway[12] with secondary electron emission representing a criticial aspect of the feedback from material surface to plasma.

*Postdoctoral Researcher, Dept. of Mechanical and Aerospace Engineering , tmatlock17@ucla.edu.
†Adjunct Professor, Dept. of Mechanical and Aerospace Engineering
‡Assistant Professor, Dept. of Mechanical and Aerospace Engineering

Initial studies of Pi facility operation revealed non-monotonic trends in the ion current delivered to a target with changes in discharge current and cathode mass flow rate.[13,14] Analytical and numerical models are being developed to better understand the origin of these trends and inform future designs and studies. A critical first step towards an analytical framework is measurement of the plasma conditions in the near anode region, where the high density plasma exits the discharge before streaming axially to a target 70 cm away. The purpose of this paper is to present the results of electrostatic probing, by emissive and double probes, in the near anode region, which marks the interface between the source and target delivery systems.

The magnetic field internal to the anode is altered to examine the corresponding changes in plasma profiles. We find distinct changes in trends at low versus high magnetic field strengths. Temporal measurements reveal that these changes are accompanied by the onset of high amplitude oscillations in floating emissive probe potentials at low frequencies (10-100 kHz). Similar fluctuations are observed in a wide variety of related plasmas and are expected to have implications on the anomalous transport of electrons across magnetic field lines.[15]

II. Experimental Apparatus

The Pi facility at UCLA is comprised of a 1.8 m diameter by 2.8 m long vacuum chamber evacuated by dual cryopumps with a combined pumping speed of 5000 L/s on argon, allowing base pressures as low as 5 x 10^{-7} Torr. The plasma source is mounted on one flange of the chamber, diametrically opposed to the flange which supports the sample manipulator arm. Intermediate guide magnets are mounted to struts lying chordally across the bottom of the chamber. All components of the plasma source and delivery system lie within the vacuum chamber with small axial gaps between system elements allowing for the insertion of plasma diagnostics in a flexible manner. A sketch of the facility layout is given in Figure 1a and a picture of plasma bombardment of a graphite target is shown in Figure 1b.

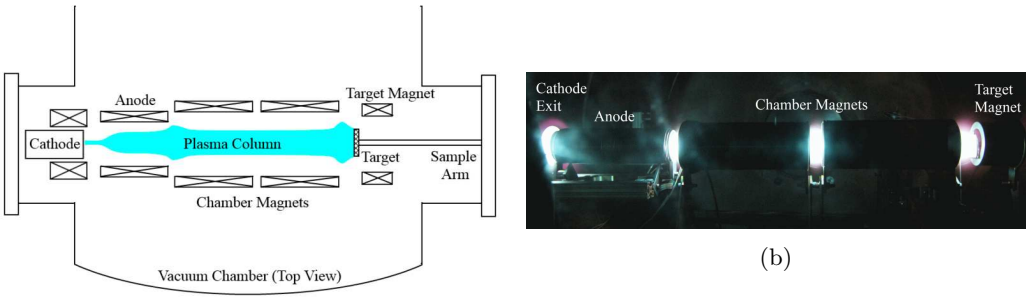

(a) (b)

Figure 1: (a) Pi facility sketch (top view) (b) Pi facility in operation on xenon (front view)

The plasma source consists of a 250-A lanthanum hexaboride (LaB_6) hollow cathode coupled to a 30 cm long, cylindrical copper anode of 6 cm inner diameter. A graphite keeper electrode positioned around the cathode tube aids in starting the discharge and helps to protect the orifice plate and graphite tube end from ion bombardment from the cathode plume plasma. A magnetic field coil positioned around the cathode and a solenoid wound on the anode provide an axial magnetic field that both confines the electrons to improve the ionization and guides the plasma to the target region.

The plasma from the source region is coupled through two 10 cm diameter chamber solenoids to a target located just upstream of a final magnetic coil. The plasma transport region through the chamber solenoids is intended to provide isolation between the target being sputtered and the plasma source. The ionization mean free path for particles sputtered from the target is typically less than the distance from the target to the anode, and the ions created from the target material then diffuse to the walls of the solenoid spools or fall back down the axial potential gradient in the plasma to the target region. Similarly, the dense plasma in the anode region rapidly ionizes particles sputtered from cathode surfaces, which are recycled their and thus segregated from the target region.

The plasma source components (anode and cathode) float relative to the vacuum facility and the grounded

chamber solenoids. Because of the large area of the grounded solenoids, the plasma tends to float within an electron temperature of the ground potential over the entire range of discharge currents. Since the bias applied to the target is made relative to chamber ground, this provides a stable reference potential from which the ions are accelerated through the sheath to the biased sample. A more detailed description of the device is provided elsewhere.[13,14]

A. Plasma Diagnostics

Plasma potential profiles near the anode are measured (up to a near unity factor of electron temperature) by a floating emissive probe. The electron temperature is then measured in the same location with a floating, asymmetric double probe. An analytical technique allows estimates of the plasma density and potential from the double probe as well, with potential profiles generally matching those found using the emissive probe. The double probe has been chosen for this experiment due to the high power deposition expected for a single probe collecting electron saturation current in the dense, near anode plasma.

1. Emissive Probe

The floating emissive probe consists of a 6.35 mm diameter tube of double bore alumina with a 0.13 mm diameter tungsten filament attached to tantalum leads and protruding in a roughly 5 mm diameter semicircle. The filament is heated by a floating DC power supply and the floating potential measured with a time resolution of up to about 100 kHz using the circuit of Figure 2a. An LT1055 op-amp is used as a unity gain buffer to lower the output impedance of the floating potential measurement and increase the bandwidth capability of the DAQ, a National Instruments PCI-6363.

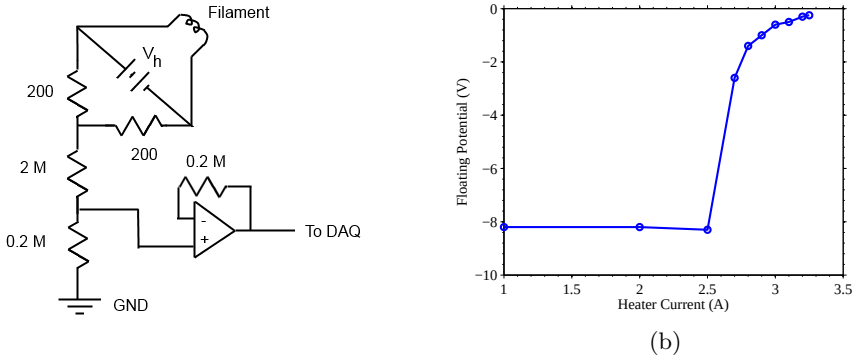

(a) (b)

Figure 2: (a) Floating emissive probe circuit. (b) Floating emissive probe potential versus heating current to the filament taken near the anode edge with Pi operating at a 55 A discharge current.

As the emissive probe is heated past a threshold temperature it begins to emit an electron current, causing it to float at a potential closer to that of the surrounding plasma. When the probe is emitting enough electrons the plasma sheath becomes space charge saturated and no further electron current can be drawn from the filament to the plasma. At saturation the probe floats a factor near unity of the electron temperature below the plasma potential. One can then monitor the floating potential of an emissive probe heated well into the space charge saturated limit in order to estimate the local plasma potential if the electron temperature (and the near unity factor) is known.

According to the 1-dimensional analysis of Hobbs & Wesson, an electrode emitting a space charge limited electron current will float to a potential $1.02T_e$ below the plasma potential for a xenon plasma.[16] Fruchtman, Zoler & Mankrinich calculate the potential of a space charge saturated, electron emitting, cylindrical probe with a finite sheath size,[17] using the Allen-Boyd-Reynolds theory. They find that a probe will float, in a

high atomic number plasma, from $1.59T_e$ below the plasma potential when the probe is much larger than the sheath (this is $1.02T_e$ below the potential at the sheath entrance as found by Hobbs & Wesson) to $0.5T_e$ when the probe radius is roughly twice the Debye length (λ_D). Double Langmuir probe measurements described here suggest that our emissive probe radius is never less than $1.7\lambda_D$ during these experiments and is typically several times larger. We add a constant factor of $1T_e$ to the floating potential measured by the emissive probe to find an estimate for the plasma potential, which splits the possible range calculated by Fruchtman *et al* and corresponds to a probe radius of roughly $10\lambda_D$ based on their results. The uncertainty of the plasma potential measurements, based on this method, is estimated to be $+0.5T_e$ (corresponding to the upper bound for λ_D) and $-1T_e$ (accounting for possible operation below saturated electron emission by $\sim 0.5T_e$).

The dependence of the emissive probe floating potential on applied heating current is used to judge the degree of saturation. An example of such a curve is shown in Figure 2b, which shows the floating potential changing at a rate of about 1 V/A at heater currents above 3 A. We use a constant heater current of 3.25 A in an attempt to maintain space charge saturated emission at all conditions without overstressing the filament (which was found to break immediately at currents exceeding about 3.5 A). Saturation of the probe is not assured at all plasma conditions and if a strong magnetic field component exists parallel to probe holder the unmagnetized theory we apply should not be expected to hold. However the floating emissive probe technique is widely utilized[18] for its simplicity and low level of impact on the surrounding plasma compared to a Langmuir probe swept to electron saturation. The normal theory is expected to apply well in our experiment where the magnetic field is largely perpendicular to the probe and the ion drift speed is low.

2. Asymmetric Double Probe

Electron temperature measurements are obtained using an asymmetric double Langmuir probe. The double probe is made up of 0.127 and 0.254 mm diameter tungsten wires inserted into a 1.6 mm outer diameter double bore alumina insulator with 4 mm diameter holes. The tungsten wires have exposed lengths of approximately 3 mm and are separated roughly 0.6 mm. Initially, a ceramic paste was added to the face of the alumina holder to prevent stray current collection through the oversized bores, however this was found to cause a red glow from the location of the paste during plasma bombardment, with probe traces showing clear signs of contamination.[19] Subsequent probes are manufactured without paste, resulting in apparently clean current-voltage characteristics (i.e. a single maximum in the slope), and measurements indicating the plasma sheath is typically large enough to bridge the gaps between alumina and electrode.

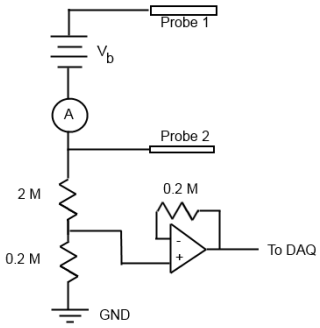

(a)

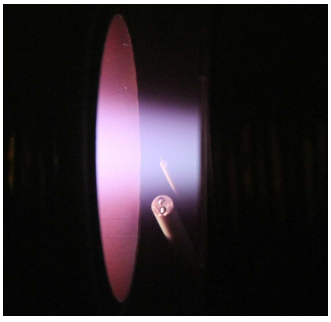

(b)

Figure 3: (a) Floating double probe circuit. (b) Double probe (top) and emissive probe (bottom) probing the near anode plasma at a low discharge current of 15 A.

The use of a double probe is motivated by the high heat flux expected near the anode where radial electron currents may exceed 1.5 kA/m^2. A large differential voltage may be applied without either electrode collecting more electron current than the ion saturation current collected by the other electrode, ensuring low levels of probe heating without the need for rapid translation. These probes are also minimally invasive,

since the electrodes float with respect to the plasma potential and never draw excessive currents from the plasma. The probe circuit, shown in Figure 3a, is similar to that utilized for the emissive probe. Both probes are shown in the near anode plasma in Figure 3b, with the discharge run at a low setting of 15 A.

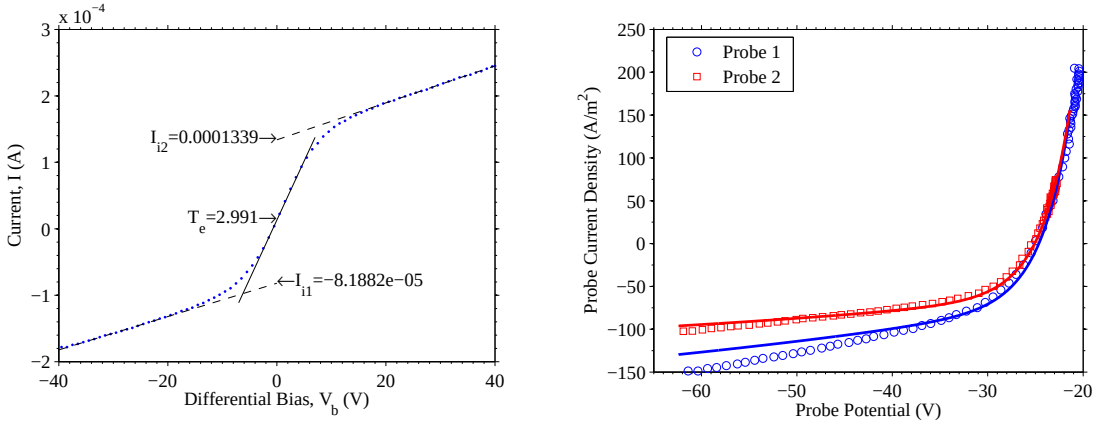

(a) (b)

Figure 4: (a) Example double probe current-voltage characteristic demonstrating the Equivalent Resistance Method (b) Double probe trace split into current-voltage curve for each of the two electrodes. Solid lines are the result of least squares fitting using Chen's parametrization of Laframboise theory. Probe 2 has the larger area so ion collection is less dependent on potential.

An apparently new technique is utilized which allows us to obtain plasma density and potential estimates along with the electron temperature measurements for which double probes are often purposed. This technique, which is an amalgamation of previous methods, will only be discussed briefly here, with further details and discussion planned for a forthcoming publication. Our method relies on parametrized Laframboise curves to match the ion current collected as a function of probe voltage below the local plasma potential by electrodes with different values of probe radius to Debye length ratio, $\xi = r_p/\lambda_D$,. The Laframboise theory of ion collection for arbitrary probe size has been applied to double probe analysis in the past by Beal *et al*,[20] with the primary distinction here being the use of an asymmetric probe resulting in a minimization problem for two values of ξ.

A simple method for analyzing a small asymmetric double probe is outlined here, where the electron temperature is first estimated using the Equivalent Resistance Method of Johnson & Malter,[21] where the ion saturation currents are estimated by linear extrapolation to zero differential bias (i.e. the floating potential of either electrode). An example application of this method is given in Figure 4a where the electron temperature, T_e, is calculated based on extrapolated ion currents, I_{i1} and I_{i2}, to probes 1 and 2 respectively, using

$$T_e = \frac{I_{i1} I_{i2}}{I_{i1} + I_{i2}} \left[\frac{dV_b}{dI}\right]_{V_b=0} \tag{1}$$

where V_b is the differential bias between electrodes and I the corresponding current. Since the floating potential of the circuit is known for each differential bias, the current-voltage characteristics can be separated for each of the two differently sized electrodes, as shown in Figure 4b where the larger radius probe (labeled as Probe 2) clearly exhibits less voltage dependence in ion saturation as predicted by the theory of Laframboise. Various fits to the curves calculated by Laframboise exist, that can be used to calculate the ion current to a cylindrical probe of some size for any probe potential with respect to the local plasma potential, with the ion density and electron temperature (which together determine λ_D in a quasineutral, 2 species plasma) as inputs. The data presented here are analyzed using the parametrization of Chen,[22] who presents a fit applicable down to ξ approaching zero. This parametrization is noted to be less accurate than similar fits applicable when $\xi > 3$, but this threshold is often passed for the smaller electrode used here.

$$\left(\frac{I_i}{I_0}\right)^{-4} = (A\eta^B)^{-4} + (C\eta^D)^{-4} \tag{2}$$

$$I_e = I_0\sqrt{\frac{m_i}{m_e}}\exp(\eta) \tag{3}$$

In Equation 2 the ion current, I_i, normalized by $I_0 = en_eA_p\sqrt{T_e/(2\pi m_i)}$, is related to the normalized probe potential, $\eta = e(V_{pl} - V_p)/T_e$ and the normalized probe radius, ξ, by fit parameters, $A - D$, which themselves depend on ξ. The fit parameters are calculated using Equation 10 and Table 4 from Chen.[22] The electron current collected by the probes is also a function of the plasma potential referenced probe bias, electron density and temperature and is taken in the usual form in Equation 3 assuming a Maxwellian distribution of electrons. Assuming away any gradients in the plasma parameters between the two electrodes, we can then apply a common minimization technique (such as Gauss-Newton or Levenberg-Marquardt) to find the values of V_{pl} and n_e (with T_e from the Equivalent Resistance method) that give the best fit of $I(\eta) = I_e - I_i$ simultaneously for the two electrodes of different ξ. An example of a least squares fit to the double probe trace of Figure 4a using Equations 2 & 3 is shown in Figure 4b with solid lines.

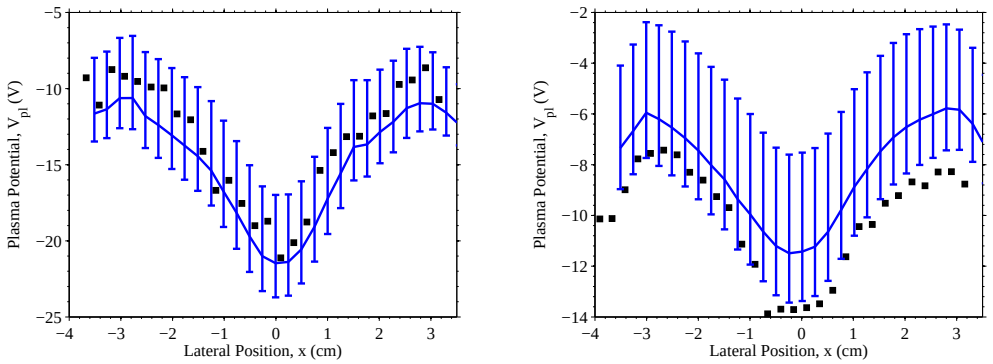

(a) (b)

Figure 5: Comparison of plasma potential profiles measured using an emissive probe (solid line) and double probe (squares) for (a) typical match and (b) poorer match

Plasma potentials calculated using this double probe methodology have been found to yield a close match to profiles measured with a floating emissive probe (corrected using the electron temperature found with the double probe). Figure 5a shows a typical case where the double probe derived potential matches the emissive probe potential within the assumed uncertainty of the emissive probe ($+1T_e/-0.5T_e$). Uncertainty in the double probe measure of potential is omitted from the figure for clarity, and is difficult to estimate in practice, though the appropriateness of each fit may be judged to some extent by the sum of the residuals squared. Figure 5b gives a comparison representative of an inexact match between the two probes, that is still quite close considering how far below the plasma potential the electrodes which make up the double probe remain. Only one case in the experiments reported here was found with a worse match between probes than that shown in Figure 5b.

The double probe only collects the most energetic electrons from the plasma as it remains biased well below plasma potential to limit the electron current to levels matching that of the ions. Thus, little information on the electron energy distribution may be obtained unless the degree of probe asymmetry is large. If the collected electrons are from a Maxwellian distribution the analysis outlined above holds, though it must be amended if this assumption is no longer valid. Though double probe application is generally limited to cases where the electron distribution is known it may be expected to be less sensitive than a single Langmuir probe to inaccuracies caused by the strong magnetic fields since it never draws more current from the plasma than ought to be available naturally to maintain quasineutrality.

The ion collection theory applied assumes the electron temperature is much higher than the ion temperature, an assumption which has not yet been verified in this device, but is estimated to hold due to low collisional energy exchange between ions and electron. Additionally, it is assumed that the plasma electron and ion densities are equal, though this may be inaccurate near the axis where the energetic electrons emitted from the cathode may represent a significant fraction of the total electron density.

III. Near Anode Plasma Measurements

Experiments described here apply constant neutral xenon flow rates of 6 sccm injected through the cathode and 14 scccm through the auxiliary ring injector just upstream of the anode, resulting in a 1 x 10^{-4} Torr pressure in the surrounding vacuum chamber (corrected for xenon). Plasma parameter profiles measured across the vertical center of the device, approximately 1 cm downstream of the anode exit are shown in Figures 6b & 7 for various values of current applied to the anode solenoid. The discharge is run at 55 A with cathode, chamber and target magnets set to solenoid currents found to maximize ion flux to the target at higher discharge currents ($\sim$ 100 A) for continuity with prior testing.[13] Discharge voltages necessary to maintain a 55 A current naturally increase as the anode magnetic field becomes stronger, as demonstrated in Figure 6a, with the majority of the increased voltage manifest in cathode potentials, V_c, further below ground, though the potential of the anode, $V_a = V_c + V_d$, is elevated further from ground as well.

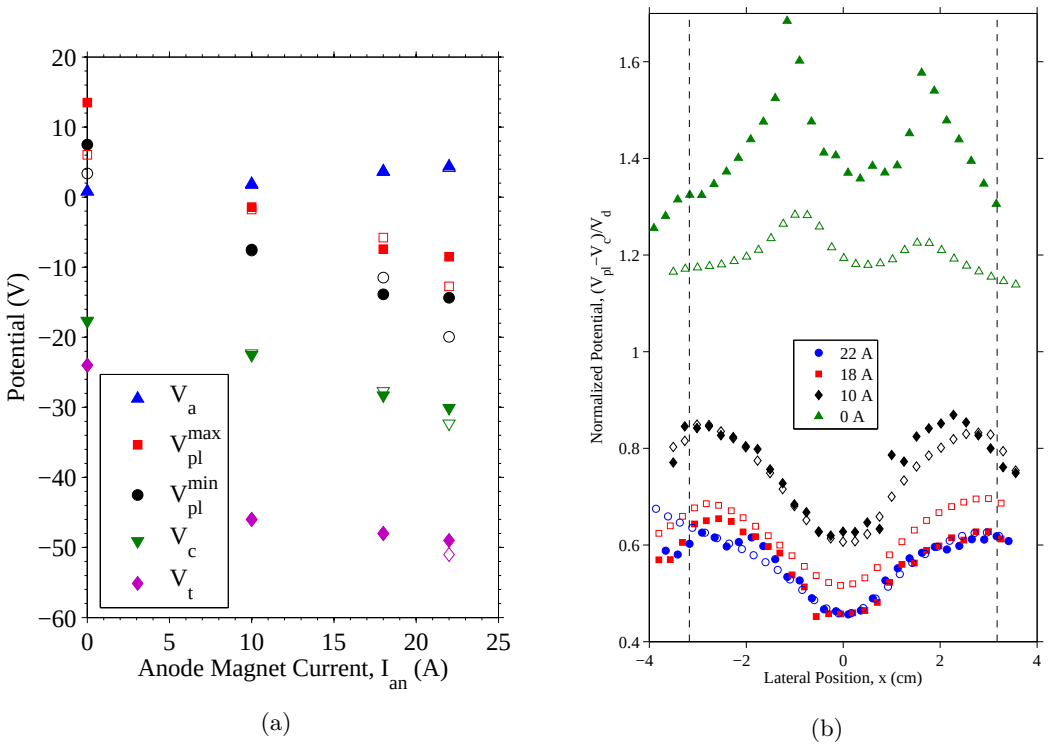

(a) (b)

Figure 6: (a)Potentials of the anode, cathode, target (floating) and extrema of the plasma potential profiles measured near the anode by double probe (filled) and emissive probe (open) as the magnetic field strength in the anode is altered. (b) Profiles of plasma potential from double probe (filled) and emissive probe (open) measurements for different anode magnet currents. Dashed lines coincide with anode inner diameter.

Plasma potential measurements, plotted in Figure 6b where they are referenced to the cathode and normalized by the discharge voltage, reveal a distinct profile in the case where the anode coil is de-energized, with all measured potentials above that of the anode (which floats <1 V above ground in this case). Even with no current to the anode magnet the magnetic field strength on axis near the probe is around 70 G so that the electron larmor radii are still less than 1 mm for electrons of moderate energy. This field is due to the high coil currents still under application to the cathode and chamber solenoids adjacent to the anode, which maintain a strong field near the probe though the field around the axial center of the anode drops below 10 G (as shown in simulations in the Appendix).

Field lines connect the outer radius of the cathode exit orifice to the anode walls, at this setting, so the plasma may be expected to float above the anode in order to meter the rapid loss of electrons along field lines. A somewhat unexpected feature of the plasma potential profiles measured in this case is the formation of a potential well on-axis. The size of this well depends on the probe, with 6 V measured by the double probe and 2 V measured by emissive probe between the local minimum on-axis and the surrounding maxima.

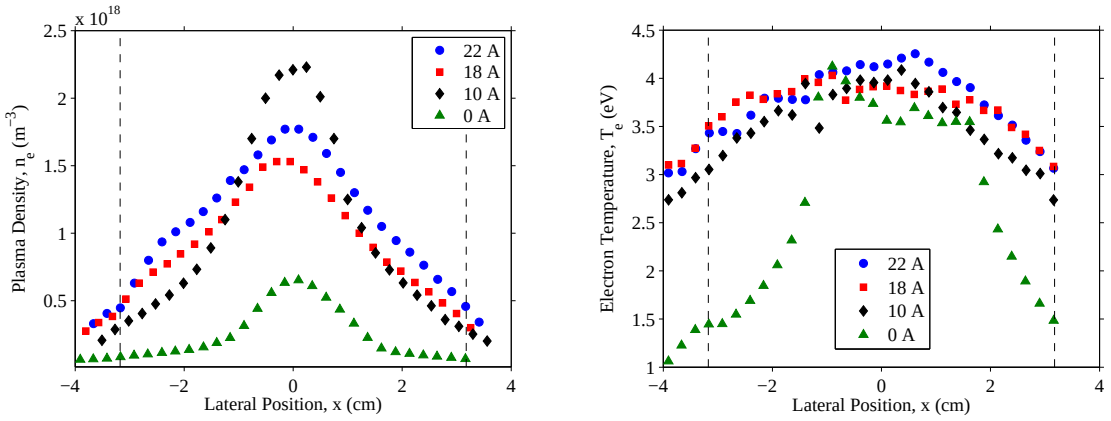

Figure 7: Profiles of (a) secondary electron density (b) electron temperature from double probe measurements for different anode magnet currents. Dashed lines coincide with anode inner diameter.

Increasing the on-axis field strength to over 100 G near the probe leads to a radial electric field which points towards the axis at all lateral positions within the anode diameter. Measured potentials lie closest to the anode when the magnetic field strength is still low, corresponding to a coil current of 10 A. Double probe results show little change between the normalized profiles at 18 A and 22 A, while the emissive probe data suggest a continual decrease with magnet current in the fraction of the discharge voltage a cathode emitted electron obtains before reaching the axial location of the probes.

Potential profiles for non-zero values of magnet current resemble those measured in common reflex arc or Penning type discharges.[23] Electrons are well confined by the axial magnetic field while ions can diffuse readily to the anode, so a radial field must form to confine ions and draw the large electron current necessary to sustain the discharge. Interestingly, the potential well on axis is close to 6 V below the maximum plasma potential at all magnetic field settings (including 0 A to the anode coil), which is roughly $3/2T_e$ in all cases as well. The on-axis potential remains 15 V above the cathode (within 1 V) for the field settings above 100 G, jumping to 25 V above cathode for the lower field strength case (according to the double probe measurements). The inversion of the potential at low magnetic field has long been a known feature of cylindrical plasmas and an analytical treatment of this effect is given by Ewald, Crawford & Self,[24] though it is for the case of ambipolar diffusion.

Ion density profiles, shown in Figure 7a, also exhibit trends that change with field strength. No anode coil current leads to a narrow (2 cm FWHM) density peak inside the region where the radial electric field points towards the axis, with a low, broad (5.7 cm FWHM) density distribution at higher radius. Increasing the anode coil to 10 A causes a dramatic increase in density everywhere (by over a factor of 3), a slight increase in the width of the inner beam and a rise in the density at high radius relative to the on-axis density. An anode magnet current of 18 A (140 G at the probes) actually results in a decrease in the density of the on-axis beam, compensated by an increase in density where $r > 2$ cm. Further increases in magnetic field strength result in a slight rise in density everywhere, with the inner beam essentially blending in with the wide density profile of the outer plasma.

The change in the relative density found on-axis compared to the anode radius may easily be expected from Figure 6a assuming the inner beam is dominated by the energetic electrons from the cathode and the outer beam is comprised of electrons created through inelastic collisions with the neutral background (with ions relatively free to fill all regions). Comparing the voltage between cathode and the on-axis plasma potential minimum with the voltage from the axis to the anode we see trends with magnet coil settings that mirror those in beam density ratios. A 0 A coil current the inner beam density is at its highest relative to the outer beam and correspondingly, the energy gained by cathode electrons is at its maximum value. From 10 to 22 A the voltage from cathode to plasma minimum is relatively constant, but the voltage from axis to cathode is steadily increasing as is the ratio of outer beam to inner beam density. The plasma electrons generated from inelastic collisions carry the cross-field current to the anode, experience higher levels of Joule heating as the magnetic field is raised, contributing to increased ionization by these secondary electrons as

they make their way to the anode.

Electron temperature profiles, shown in Figure 7b, generally exhibit a shallow minima near the axis, similar to measurements in a reflex arc,[25] with maxima occurring within 1 cm of the axis. The elevated temperatures just off axis may be due to Joule heating of the electrons by the inward pointing electric field. Measured radial temperature gradients are small (<1 eV within an anode radius) when the magnetic field is >100 G at the probes, while the temperature drops rapidly with radial location (e-folding length of ∼2 cm) when the anode magnet coil is de-energized. This rapid drop in temperature may be due to the connection of magnetic field lines directly to anode surfaces at high radial positions. A large parallel resistivity would be required to maintain high temperatures here.

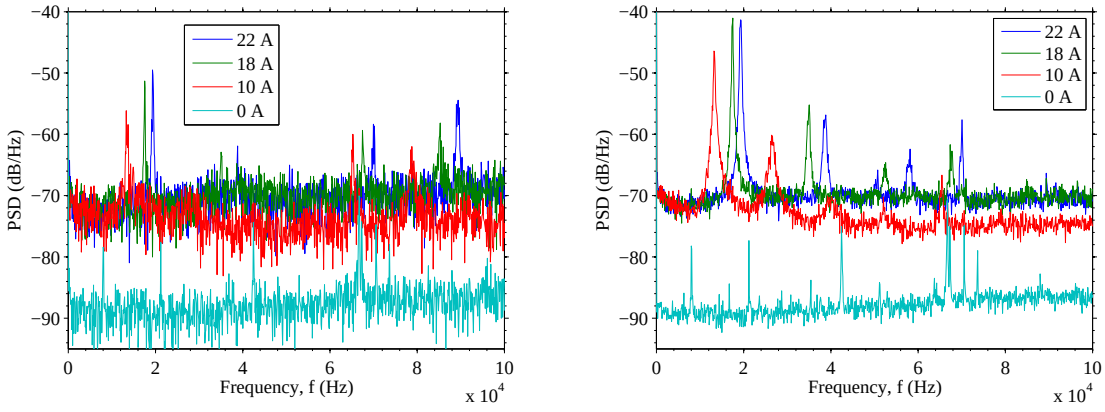

Figure 8: Power spectral densities of floating emissive probe potential for different anode magnet current settings averaged over measurements taken (a) within 5 mm of the axis and (b) 5 to 40 mm off axis.

Fluctuations in the floating potential measured on the hot emissive probe are presented in the power spectral density plots of Figure 8, where the near-axis region (r <5 mm) is separated from the outer region due to prominent differences in the spectral content. An 8-20 kHz mode, exhibiting a roughly linear frequency dependence on magnetic field strength, appears to dominate the plasma potential oscillations. These oscillations have an amplitude as high as $\pm 0.15 V_d$ with sharp peaks resulting in the second and third harmonics apparent in the spectral density plots. The amplitude of this mode appears to decrease gradually as the anode magnet current is decreased from 22 to 10 A, with a sharp drop-off in all oscillations at the lowest magnetic field strength setting tested.

The amplitude of the 8-20 kHz oscillations found at high magnetic field strength diminishes near the axis, where an 80-90 kHz mode becomes prevalent. The frequency of this higher frequency mode also appears to increase roughly linearly with anode magnet current, with lower amplitudes at low current. Another peak can be identified in the power spectral density near 70 kHz, which appears to be a beat frequency between the lower frequency oscillations dominant at high radius and the 90 kHz mode found on-axis.

The electron density gradient and radial electric fields measured are known to drive drift instabilities in reflex arc discharges,[23] however these instabilities lead to oscillation frequencies proportional to the electron azimuthal drift speed, which in our case is decreasing as the magnetic field strength is augmented. An anti-drift mode may exist, with a frequency inversely proportional to the drift speed, but the predicted frequency from our measurements of an m=1 mode of this type is about an order of magnitude lower than the 10 kHz oscillations observed. In the approximate regime relevant here, the anti-drift mode frequency is noted by Frias *et al*[26] to scale as $\omega \simeq \omega_{ci} k_\theta L_n$ where the electron density scale length is $L_n = [\partial/\partial r(\ln n_e)]^{-1} \sim 2$ cm, based on measurements shown here, and the azimuthal wavenumber is $k_\theta = 2\pi/\lambda \sim 1/(2\text{ cm})$ for an m=1 mode at the radial location of highest measured fluctuation amplitude.

The measured frequency of the 10 kHz range modes are noted to be essentially independent of the location of the measurement while the ion cyclotron frequency can vary in the measurement range by up to a factor of 2 and the drift speeds calculated from the measured profiles are non-monotonic (a strong shear exists where the radial electric field switches signs). A purely azimuthal mode ought to have a linear dispersion in our case. A possible candidate is the Modified Simon-Hoh instability measured and formulated by Sakawa *et*

al,[27] who find an oscillation with a frequency nearly an order of magnitude above ω_{ci}, independent of radial location and an increasing function of magnetic field. This mode is similar to the normal drift wave seen in cylindrical plasmas, but differs in that azimuthal charge separation is brought about by the large gyroradius of the unmagnetized ions rather than through collisional drag on the ion fluid.

The derived dispersion relation shows the frequency is nearly equal to the azimuthal transit frequency of the ions and that the instability is excited when both the ion azimuthal drift speed is lower than the ExB speed and the azimuthal electron drifts due to the radial electric field and pressure gradient are in the same direction. The condition that the electron drifts are additive for the instability to propagate may explain the cutoff observed here at low magnetic field, when the radial electric field switches signs. The experiments of Sakawa *et al* were performed in a linear device with a small discharge current collected by an axially located electrode rather than the cylindrical discharge employed here where large radial electron currents exist.

A rotational instability with similar dependence of frequency on magnetic field strength is found in the linear Mistral device and is captured in the model of Annaratone *et al*.[28] The instability is described as a connection between the central plasma column and the current collecting, radial boundary by an azimuthally finite 'arm', that begins as an m=1 mode at low magnetic field. The rotational frequency is equal to the azimuthal drift speed of ions, which is assumed to be on the same order as the electron azimuthal drift in the plasma arm. The oscillations in Pi, described here, are suspected to be due to a mechanism similar to what is found by Sakawa and Annaratone, though further measurements are required before the instability can be identified.

IV. Conclusion

Measurements of the plasma conditions near the anode of a device designed for plasma-material interactions experiments reveal large differences in trends with anode magnet field strength at low and high field settings. When the anode electromagnet is deactivated the plasma potential is always above the anode potential, with a radial electric field that switches signs near the axis of the device, to confine ions on-axis where a beam of energetic electrons emitted by the cathode is expected to persist. Increasing the magnetic field strength constricts electron collection on the anode to the point where the electric field everywhere (inside the anode radius) must act to promote the radial transport of electrons.

A narrow beam of high ion density appears to broaden, and at some point decrease in amplitude as the magnetic field strength inside the anode is raised. This result seems somewhat counter-intuitive since the magnetic field tends to have a constricting affect on the plasma, however it is explained by simple arguments based on the changes in potential differences between the cathode, the on-axis plasma and the anode. Measured electron densities near the anode of $> 10^{18}$ m^{-3} are high enough to promote redeposition of materials sputtered from cathode surfaces back to the discharge surfaces rather than contaminating target surfaces.

An alternative double probe technique described here has yielded plasma potential measurements that closely matched those found using a common emissive probe method for a majority of test conditions. This technique may provide a simply implemented method for measuring electron density, temperature, and plasma potential in a dense plasma without the need for fast translation to avoid overheating.

Additionally, oscillations in the floating potential of an emissive probe are observed which have a radial spatial dependence only very close to the axis of symmetry. These oscillations occur at low frequencies, with one band at 8-20 kHz and another at 80-90 kHz, both lying well within the range between the ion cyclotron frequency, f_{ci} $\sim$1 kHz, and the lower hybrid frequency, f_{lh} $\sim$500 kHz. The lower frequency modes are believed to be azimuthally propagating with a linear dispersion due to prevalence of plasma rotation in similar devices. Future work will be dedicated to the full spatio-temporal characterization of these oscillations. Measurements shown here will be used to validate numerical models of the device[9] which are in turn intended to inform improvements to facility design.

Acknowledgments

This work is funded by the U.S. Air Force Office of Scientific Research under grant no. FA9550-11-1-0282 and the UCLA School of Engineering and Applied Sciences. The authors would like to thank Danielle Waters, Chris Dodson, Ryan Conversano and Ben Dankongkakul for their assistance in the laboratory.

A. Appendix: Magnetic Field Simulations

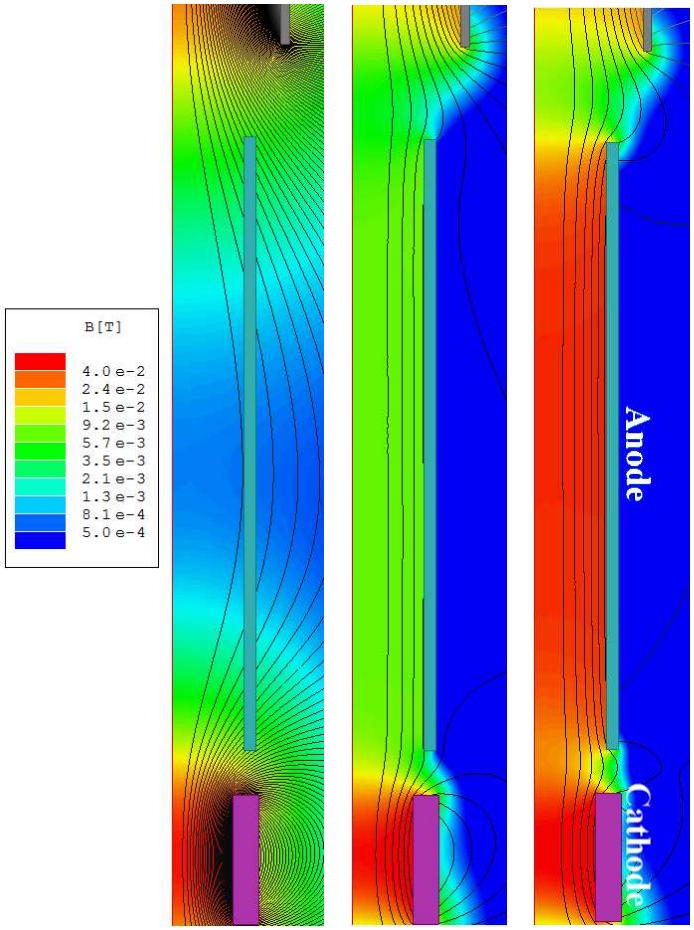

Figure 9: Maxwell simulation of magnetic field with anode magnet currents of (a) 0A (b) 10A and (c) 22A focusing on the region of the discharge.

References

[1]S Sharafat, A Aoyama, B Williams, and N Ghoniem. Development of micro-engineered textured tungsten surfaces for high heat flux applications. *Journal of Nuclear Materials*, pages 1–7, 2013.

[2]Y Hirooka, RW Conn, T Sketchley, WK Leung, G Chevalier, R Doerner, J Elverum, D M Goebel, G Gunner, and et al. A new plasma-surface interactions research facility: PISCES-B and first materials erosion experiments on bulk-boronized graphite. *Journal of Vacuum Science and Technology A*, 8(3):1790–1797, 1990.

[3]H J N Van Eck, W R Koppers, G J Van Rooij, W J Goedheer, B De Groot, P Smeets, J Scholten, M Van De Pol, S Brons, R Koch, B Schweer, N J Lopes Cardozo, and A W Kleyn. Pre-design of Magnum-PSI : A new plasma wall interaction experiment. *Fusion Engineering and Design*, 82:1878–1883, 2007.

[4]T Uckan. Plasmamaterials interactions test facility. *Review of Scientific Instruments*, 58(1):17–19, 1987.

[5]G M Wright, D G Whyte, and B Lipschultz. Measurement of hydrogenic retention and release in molybdenum with the DIONISOS experiment. *Journal of Nuclear Materials*, 390-391:544–549, 2009.

[6]D Naujoks, G Fussman, and H Meyer. I(U)-characteristics of the plasma generator PSI-1: Experiment and theory. *Contributions to Plasma Physics*, 38:127–133, 1998.

[7]B Bottin, S Paris, V Van Der Haegen, M Carbonaro, Vincent Van Der Haegen, and Mario Carbonaro. Experimental and Computational Determination of the VKI Plasmatron Operating Envelope. In *30th Plasmadynamics and Lasers Conference*, number 3607, Norfolk, VA, 1999.

[8]WP Owens, J Uhl, M Dougherty, A Lutz, J Meyers, and DG Flecther. Development of a 30 kW inductively coupled plasma torch facility for aerospace material testing. In *30th Plasmadynamics and Lasers Conference*, 1999.

[9]TS Matlock, DM Goebel, R Conversano, and RE Wirz. The Plasma Interactions Facility at UCLA. In *33rd Internation Electric Propulsion Conference*, Washington DC, 2013.

[10]SJ Araki and RE Wirz. Particle Simulation of Near-Surface Cusp Confinement of Weakly Ionized Plasma. In *33rd Internation Electric Propulsion Conference*, Washington DC, 2013.

[11]T Crosby and NM Ghoniem. Multiphysics model of thermomechanical and helium-induced damage of tungsten during plasma heat transients. *Journal of Nuclear Matlerials*, 2013.

[12]M Patino, Y Raitses, B Koel, and RE Wirz. Application of Auger Spectroscopy for Measurement of Secondary Electron Emission from Conducting Material for Electric Propulsion Devices. In *33rd Internation Electric Propulsion Conference*, Washington DC, 2013.

[13]TS Matlock, DM Goebel, R Conversano, and RE Wirz. The Plasma Interactions Facility at UCLA. In *49th AIAA/ASME/SAE/ASEE Joint Propulsion Conference and Exhibit*, San Jose, CA, 2013.

[14]TS Matlock, DM Goebel, R Conversano, and RE Wirz.

[15]W. Horton. Drift waves and transport. *Reviews of Modern Physics*, 71(3):735–778, April 1999.

[16]GD Hobbs and JA Wesson. Heat flow through a Langmuir sheath in the presence of electron emission. *Plasma Physics*, 9:85–87, 1967.

[17]A. Fruchtman, D. Zoler, and G. Makrinich. Potential of an emissive cylindrical probe in plasma. *Physical Review E*, 84(2):025402, August 2011.

[18]J. P. Sheehan, Y. Raitses, N. Hershkowitz, I. Kaganovich, and N. J. Fisch. A comparison of emissive probe techniques for electric potential measurements in a complex plasma. *Physics of Plasmas*, 18(7):073501, 2011.

[19]Brian a. Smith and Lawrence J. Overzet. Improvements to the floating double probe for time-resolved measurements in pulsed rf plasmas. *Review of Scientific Instruments*, 69(3):1372, 1998.

[20]Brian Beal, Lee Johnson, Daniel Brown, Joseph Blakely, and Daron Bromaghim. Improved analysis techniques for cylindrical and spherical double probes. *The Review of scientific instruments*, 83(7):073506, July 2012.

[21]EO Johnson and L Malter. A floating double probe method for measurements in gas discharges. *Physical Review*, 80(1):58–68, 1950.

[22]Francis F. Chen. Langmuir probe analysis for high density plasmas. *Physics of Plasmas*, 8(6):3029, 2001.

[23]EB Jr Hooper. A Review of Reflex and Penning Discharges. *Advances electronic & electron physics*, 27:295, 1970.

[24]H N Ewald, F W Crawford, and S A Self. Steady-State Theory of an Intermediate-Pressure Discharge Column in a Magnetic Field. *Journal of Applied Physics*, 38(7), 1967.

[25]FF Chen. Radial electric field in a reflex discharge. *Physical Review Letters*, 8(6):234–237, 1962.

[26]Winston Frias, Andrei I. Smolyakov, Igor D. Kaganovich, and Yevgeny Raitses. Long wavelength gradient drift instability in Hall plasma devices. II. Applications. *Physics of Plasmas*, 20(5):052108, 2013.

[27]Y Sakawa, C Joshi, P K Kaw, F F Chen, and V K Jainb. Excitation produced of the modified plasma instability in an electron beam produced plasma. *Physics of Fluids B*, 5(6):1681, 1993.

[28]B. M. Annaratone, a. Escarguel, T. Lefevre, C. Rebont, N. Claire, and F. Doveil. Rotation of a magnetized plasma. *Physics of Plasmas*, 18(3):032108, 2011.